Kinetically controlled vapor-diffusion synthesis of novel nanostructured metal hydroxide and phosphate films using no organic reagents

Birgit Schwenzer,[a] Kristian M. Roth,[a] John R. Gomm,[a] Meredith Murr[b] and Daniel E. Morse*[ab]

Received 12th September 2005, Accepted 31st October 2005
First published as an Advance Article on the web 18th November 2005
DOI: 10.1039/b512900a

Nanostructured $Co_5(OH)_8Cl_2{\cdot}3H_2O$, $Co_5(OH)_8(NO_3)_2{\cdot}2H_2O$, $Co_5(OH)_8SO_4{\cdot}2H_2O$, $Zn_5(OH)_8(NO_3)_2{\cdot}2H_2O$, $Cu_2(OH)_3(NO_3)$ and $Mn_3(PO_4)_2{\cdot}7H_2O$ thin films have been prepared using a kinetically controlled vapor-diffusion method. Vectorial control by diffusion of ammonia as a base catalyst into an aqueous metal salt solution yields large area (2 cm^2) metal hydroxide and metal phosphate films with unique structures. No supporting substrate for growth of the films is necessary in this approach. The films were characterized using X-ray powder diffraction and scanning electron microscopy. The cobalt containing films were studied in more detail using transmission electron microscopy, X-ray photoelectron spectroscopy, X-ray absorption near edge structure and various chemical analysis techniques. For the first time the electronic properties and crystal structure of these materials could be studied in thin films not influenced by the presence of an underlying substrate. For $Co_5(OH)_8(NO_3)_2{\cdot}2H_2O$ films, which crystallize in a layered hydrotalcite-like structure that is homogeneous from the nanoscale to the macroscale, unprecedented photoconductivity properties were observed. Resistivity measurements show that this material is a p-type semiconductor with an unusually long minority carrier lifetime and high carrier density.

Introduction

Synthesis of nanostructured thin films has attracted increasing attention in recent years[1,2] due to their potentially superior electronic and optical properties compared to those of the corresponding bulk materials. The application of semiconducting thin films in electro-optical devices,[3] solar cell technology[4] or gas sensors[5] requires high purity, defect-free material. Most thin films are prepared by epitaxially growing the material on a substrate. Crystal lattice mismatch between the substrate and the epitaxially grown material generates defects that degrade the electronic properties of the film. Incorporation of carbon impurities, originating from the use of organometallic precursor molecules or organic solvents, can also degrade the performance.

Alternative routes to high purity semiconductor materials to replace techniques such as cost-intensive metal organic chemical vapor deposition (MOCVD), molecular beam epitaxy (MBE), and liquid phase epitaxy (LPE) are being explored in response to demands for more flexible and lower energy synthesis strategies.

Techniques that mimic biomineralization have received much attention because of the inherently benign conditions of biological syntheses. In addition, these biomineralization processes often produce highly ordered structures on the nanoscopic as well as the macroscopic scale. Examples of inorganic nanostructures prepared include the formation of nanocrystalline TiO_2[6] and Ga_2O_3.[7] In these studies, silicatein (a catalytically active, structure-directing enzyme[8]) was used as a catalyst and template for the hydrolysis and subsequent polycondensation of water stable molecular complexes of titanium and gallium to form nanocrystalline TiO_2[6] and Ga_2O_3,[7] respectively. However, the resulting nanoparticles remain in intimate contact with the macroscopic (2 μm × 1 mm) protein filaments that catalyzed and templated their synthesis; they are therefore largely unsuitable for device applications that require high purity material.

We report here a kinetically controlled vapor-diffusion synthesis of inorganic thin films. This method uses the following principles borrowed from biomimetic synthesis routes:[6,7]

a) slow catalysis of synthesis from molecular precursors provides the opportunity for kinetic control; and

b) crystal growth is vectorially regulated by a template, operating in concert with kinetic control to provide spatial and temporal control of crystal polymorph, orientation and morphology.

To capture the advantage of the slow catalysis and anisotropic, vectorial control of biocatalytic crystal growth, we developed a low-temperature, solution-based method employing the slow diffusion of ammonia vapor as a catalyst for hydrolysis of metal-containing molecular precursors. This diffusion through a solution of molecular precursor establishes a spatially and temporally regulated gradient of the catalyst, while the vapor–liquid interface serves as a nucleation template. The resulting vectorially controlled combination of the molecular precursor and hydrolysis catalyst at room temperature yields a nanostructured thin film at the vapor–liquid interface, formed as the gaseous catalyst dissolves in an

[a]*Institute for Collaborative Biotechnologies, California NanoSystems Institute and the Materials Research Laboratory, University of California, Santa Barbara, CA 93106, USA. E-mail: d_morse@lifesci.ucsb.edu*
[b]*Department of Molecular Cellular and Developmental Biology, University of California, Santa Barbara, CA 93106, USA*

aqueous metal salt solution to initiate hydrolysis. The diffusion of the basic catalyst (ammonia) into the aqueous solution creates a pH gradient that determines the morphology of the growing film, resulting in a unique structure of the film.[9] This morphology was previously reported for similar cobalt hydroxide materials by Hosono *et al*.[9] However, the methodology described here proves widely applicable for the growth of relatively large area (2 cm^2) thin films suitable for structural and electronic characterization of a number of different materials, and offers the potential of growing even larger films for device applications.

We here demonstrate the feasibility of characterizing the electronic properties of these self-supporting films and illustrate the high quality of the prepared material by describing the properties of the three different cobalt hydroxide nanostructured films, materials that have received increasing scientific interest in recent years.[9–16] $Co(OH)_2$ is used as an additive in numerous industrial processes and has potential for applications as an oil additive[17] and in alkaline secondary batteries;[18] it also displays interesting magnetic properties.[10,16] It exists in two phases: α-$Co(OH)_2$[10,16,19] and the much more common β-$Co(OH)_2$.[15,20] The cobalt hydroxide thin films prepared in this study are α-$Co(OH)_2$ materials. We also describe use of the vapor diffusion method for the preparation of zinc hydroxide, copper hydroxide and manganese phosphate thin films.

Experimental

All starting materials used in this study were commercially available and used without further purification. Two beakers, one containing a dilute solution of NH_4OH (0.7%–1.2%, depending on the experimental conditions) and one containing a separate solution of either aqueous 0.1 M $CoCl_2$, 0.1 M $Co(NO_3)_2$, 0.1 M $CoSO_4$, 0.1 M $Zn(NO_3)_2$ or 0.1 M $Cu(NO_3)_2$ were placed in the same enclosed chamber. The synthesis of metal hydroxide thin films occurred at room temperature and ambient pressure over the course of 18 h.

For the preparation of $Mn_3(PO_4)_2{\cdot}7H_2O$, 0.058 g of $(NH_4)_2HPO_4$ (0.5 equiv.) was added to 4 ml of 0.1 M $MnCl_2$ solution. The beaker containing this mixture was then exposed to ammonia vapor from a dilute solution of NH_4OH (0.7%) in a separate beaker, enclosed within the reaction chamber. The metal phosphate thin film formed at room temperature and ambient pressure over the course of 18 h. After formation, the metal hydroxide or phosphate films were transferred onto a doubly distilled water surface to remove traces of starting material solution, using the Langmuir–Blodgett technique.

For the conversion of metal hydroxides to metal oxides, approximately 0.05 g of flakes of the metal hydroxide film ($Co_5(OH)_8(NO_3)_2{\cdot}2H_2O$ or $Zn_5(OH)_8(NO_3)_2{\cdot}2H_2O$) were placed in an alumina crucible and this was loaded into a 2.5 cm diameter tube furnace. The material was then heated under air at 400 °C and 300 °C, respectively, for 4 h.

Scanning electron microscopy (SEM) was performed on dried samples using a Tescan Vega 5130 SEM. Powder X-ray diffraction (XRD) was performed using a Bruker D8 diffractometer with monochromatic Cu Kα radiation (λ = 1.540 Å). To confirm elemental composition, X-ray photoelectron spectroscopy (XPS) was performed using a Kratos Axis Ultra with a monochromated aluminium anode. Binding energy of C 1s in all spectra was shifted to 285 eV. X-Ray absorption near edge spectroscopy (XANES); Co-K-edge EXAFS spectra were collected at the Stanford Synchrotron Radiation Laboratory (SSRL) beam line 11-2 under SPEAR3. Samples were diluted to 10 wt% in boronitride (BN) and placed in a plastic (PCTFE) sample holder using Kapton tape as the window material. The X-ray energy was selected using a Si(220) double-crystal monochromator, detuned 50% for harmonic rejection. Energy was calibrated by defining the first derivative peak of a Mn metal foil to be 6540 eV. Inductively coupled plasma atomic emission spectroscopy (ICP-AES) was performed using a TJA High Resolution IRIS ICP Atomic Emission Spectrometer. Solutions of $CoCl_2$, $Co(NO_3)_2$ and $CoSO_4$, respectively, in 2% HNO_3 containing 60 ppm Co were used as the respective standards for calibration of the ICP measurements. Transmission electron microscopy (TEM) was performed using a Tecnai T20 and electron diffraction patterns were acquired at a camera length of 650 mm. UV/Vis spectra of samples dried on glass slides were taken with a Molecular Probes UV/Vis spectrometer with 2 nm resolution.

Continuous sheets of product were transferred to a platinum interdigitated array of electrodes (IDE) with a width and spacing of 5 μm. The material on the electrode was dried at room temperature under vacuum (762 mmHg) for 12 hours. The IDE was connected to a Keithley 4200 SCS testing system for *IV* and photoconduction analyses. For *IV* analysis the voltage was ramped from −0.75 to 0.75 V while monitoring the current passing through the device. Photoconductivity was observed by applying 2.5 V of bias while continuously monitoring the current through the device in the dark. The device was then exposed to visible light pulses of 2 s duration using a fiber optic light source (Ehrenreich Ind. Garden City, NY) to minimize the amount of sample heating. The light source provided an average intensity of 80 × 10^3 lux with a spectral range of 400–1400 nm.

Results and discussion

We have used the described kinetically controlled vapor-diffusion synthesis route to prepare metal hydroxide films from aqueous $CoCl_2$, $Co(NO_3)_2$ and $CoSO_4$, $Zn(NO_3)_2$ and $Cu(NO_3)_2$ solutions, as well as metal phosphate thin films (*e.g.* $Mn_3(PO_4)_2{\cdot}7H_2O$) from the appropriate precursors. The area of continuous films grown by this method depends on the diameter of the reaction vessel used. In this study the largest area of continuous film grown was ∼50 cm^2. The largest inorganic films, however, broke when transferred onto glass slides using the Langmuir–Blodgett technique and cracked further during the subsequent drying process. The overall mechanical stability of the films varies with the composition of the films, *e.g.* $Zn_5(OH)_8(NO_3)_2{\cdot}2H_2O$ and $Mn_3(PO_4)_2{\cdot}7H_2O$ are more robust and less prone to cracking during the drying process than the cobalt- and copper-containing films. The largest continuous film we used for electronic characterization thus far was ∼2 cm^2 ($Co_5(NO_3)_2(OH)_8{\cdot}2H_2O$).

Surface tension at the air–water interface and the induced pH-gradient provide a template that directs the growing materials to adopt a continuous sheet morphology. Scanning electron microscopy (SEM) images of the resulting hydroxide and phosphate films are shown in Fig. 1.

All of these materials show similar morphologies: a continuous backplane parallel to the air–water interface with plates that grow orthogonally from the backplane into the aqueous solution. Kinetic studies revealed that the crystalline plates, orthogonally oriented into the aqueous solution with respect to the common backplane, form after initial island nucleation and during consolidation of the crystalline film at the gas–liquid interface. The density, size and shape of these orthogonal plates, as well as the size of the crystalline domains, depend on the choice of the metal salt precursor and the reaction time.

This unique morphology of macroscopic and microscopic organization of the material was previously reported only by Hosono *et al.*[9] in their study of $Co(OH)_2$ films. But their method, involving growth on glass substrates with urea and methanol as reagents, yielded material with a composition of $Co(OH)_{0.93}(NO_3)_{0.03}(CO_3)_{0.52}{\cdot}0.27H_2O$,[9] revealing the stoichiometric incorporation of carbon, which is in marked contrast to the results reported here. No organic reagents or solvents were used to prepare the inorganic thin films displayed in Fig. 1.

The cobalt hydroxide and zinc hydroxide films, shown in Fig. 1a and c, respectively, were dehydrated and converted to the corresponding metal oxide films by heating in air. Complete conversion to the metal oxide was confirmed by XRD. No change in morphology could be detected by SEM (pictures not shown).

In the following section we will describe in detail the characterization of three cobalt hydroxide films prepared from different metal salt precursors. These self-supporting films—prepared by the kinetically controlled vapor-diffusion process—also proved suitable for the characterization of electronic properties, as described below.

The cobalt hydroxide films were prepared from three different precursor solutions: $CoCl_2$, $Co(NO_3)_2$ and $CoSO_4$; the respective products are designated (**I**), (**II**) and (**III**). Films prepared from these three precursor solutions show similar morphologies. In all cases the plates on the roughened side of the thin film (plates growing into the aqueous solution, Fig. 1a) are approximately 50 nm thick, 3–5 μm tall, depending on the reaction time, and randomly oriented perpendicular to a 1 μm thick backplane.

Powder XRD patterns of the ground films (Fig. 2) indicate a monoclinic crystal structure (*C*2/*m*) of α-$Co(OH)_2$ for all three products (**I**, **II**, **III**). The literature suggests that α-$Co(OH)_2$ is a molecular composite of cobalt-containing crystalline layers, rather than a single defined compound.[16,18,19] These layers

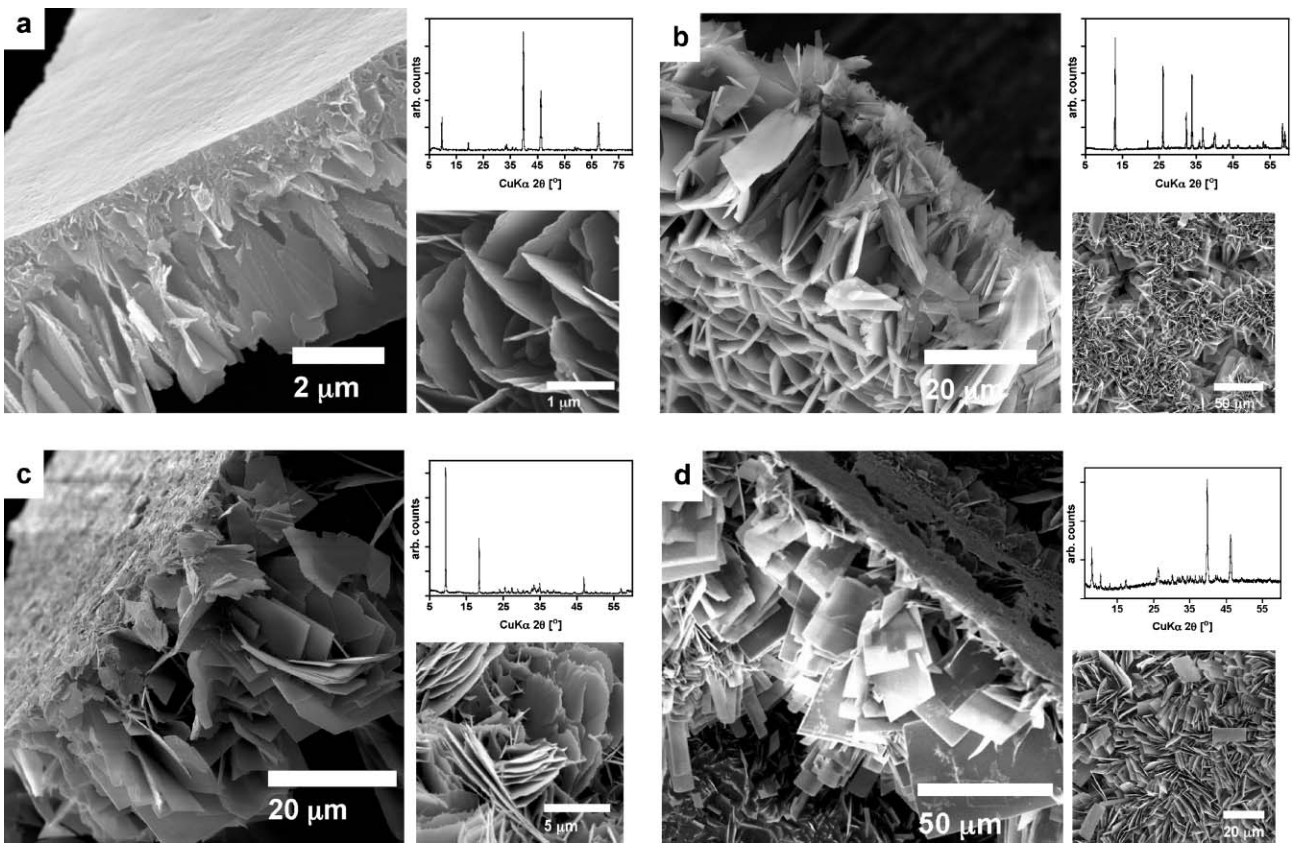

Fig. 1 Morphological and crystallographic characterization of metal hydroxide and phosphate thin films. Scanning electron microscopy (SEM; side- and bottom-view) images and XRD patterns of (a) $Co_5(OH)_8(NO_3)_2{\cdot}2H_2O$ (hydrotalcite-like structure), (b) $Cu_2(OH)_3(NO_3)$ (rouaite structure), (c) $Zn_5(OH)_8(NO_3)_2{\cdot}2H_2O$ (hydrotalcite-like structure) and (d) $Mn_3(PO_4)_2{\cdot}7H_2O$ (switzerite structure). Peaks at 39.7° and 46.2° in the XRD spectra of (a) and (d) result from the Pt holder of the instrument.

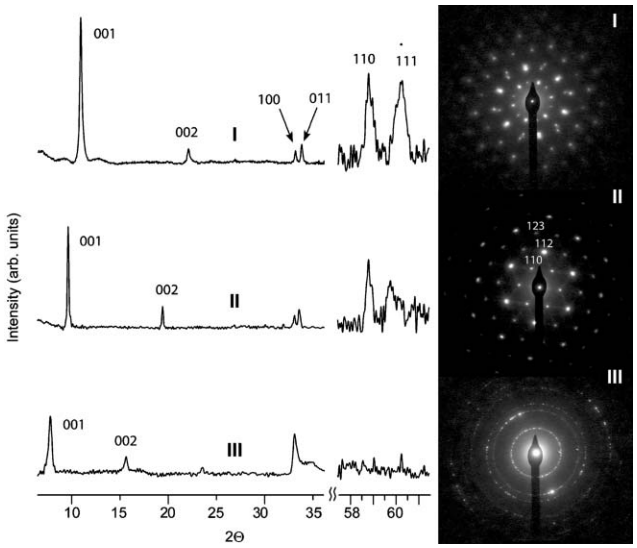

Fig. 2 Powder XRD and electron diffraction patterns for **I**, **II**, and **III** showing peaks indexing to the hydrotalcite-like structure with $a_{\mathbf{I,II,III}}$ = 3.13 Å; $c_{\mathbf{I}}$ = 8.12 Å; $c_{\mathbf{II}}$ = 9.19 Å; and $c_{\mathbf{III}}$ = 11.26 Å. Electron diffraction patterns showing only **II** is single crystalline whereas **I** and **III** exhibit varying degrees of polycrystallinity. XRD spectra are magnified by 10× after the break in 2Θ. Electron diffraction index labels belong to the spots immediately below the text.

have a net positive charge and are held together by incorporated counter ions. The net positive charge of the individual layers has been attributed to a hydroxyl deficiency within the cobalt-containing sheets of $Co(OH)_2$ which in some cases is explained by the presence of mixed valent octahedrally coordinated cobalt ions (2+ and 3+) in those layers.[9,14] The mineral hydrotalcite ($Mg_6Al_2(CO_3)(OH)_{16}\cdot 4H_2O$) displays a similar layered crystal structure in which sheets with mixed valence metal ions (2+, 3+) are coordinated octahedrally and the positively charged sheets held together by counter anions (CO_3^{2-}). Therefore the α-$Co(OH)_2$ structure is often referred to as a hydrotalcite-like structure.

Kurmoo, however, showed in a study involving X-ray absorption near edge structure (XANES) that for $Co_2(OH)_3(NO_3)$, $Co_5(OH)_8(C_7H_{15}CO_2)_2\cdot 4H_2O$ and $Co_5(OH)_8(C_2N_3)_2\cdot 6H_2O$ the positive charge of the $Co(OH)_2$ sheets results from the incorporation of tetrahedrally coordinated Co^{2+} ions into the crystal structure.[10] In a related system, $Zn_5(NO_3)_2(OH)_8\cdot 2H_2O$ crystallizes in a hydrotalcite-like structure in which the net positive charge of the Zn^{2+} containing sheets results from the incorporation of tetrahedrally coordinated ions into the crystal structure of otherwise octahedrally coordinated ions.[21]

Our findings by powder XRD are in agreement with Stählin and Oswald's reports for $Zn_5(OH)_8(NO_3)_2\cdot 2H_2O$[21] and also with the works by Kurmoo on layered α-$Co(OH)_2$ compounds.[10,16]

Well resolved (001) and (002) reflections in the XRD patterns (Fig. 2) demonstrate an increased interlayer spacing along the *c*-axis of the crystal structure in comparison to β-$Co(OH)_2$ (c = 4.6 Å[15]). The lattice parameter value in the *c*-direction for $Co_5(NO_3)_2(OH)_8\cdot 2H_2O$ (**II**, $c_{\mathbf{II}}$ = 9.19 Å) is in good agreement with previous reports (c = 8.4 Å[9]) of α-$Co(OH)_2$ thin films prepared with nitrate incorporation between the Co^{2+} containing layers. We observe a progressive increase of the interlayer spacings with increasing anion size in the order Cl^- ($c_{\mathbf{I}}$ = 8.12 Å) < NO_3^- ($c_{\mathbf{II}}$ = 9.19 Å) < SO_4^{2-} ($c_{\mathbf{III}}$ = 11.26 Å). While this trend had been reported before by Rajamathi *et al.*[19] for anion incorporation into α-$Co(OH)_2$ powder, the *c*-axis lattice spacings they report are up to ~13% smaller. However, not too much should be interpreted from this difference, since Rajamathi[19] *et al.* analyzed less crystalline materials with a different water content than reported here.

As expected, 2-D reflections [(10*l*) and (11*l*)] in the XRD pattern (Fig. 2) agree with the lattice parameters of β-$Co(OH)_2$ (a layered brucite structure, without any anion incorporation between the cobalt-containing layers[15,20]) and do not shift with changes in interplanar lattice spacings as they contain no *c*-axis component. Reflections corresponding to (111) and (011) show small shifts in *d*-spacing with respect to β-$Co(OH)_2$ again consistent with the larger *c*-axis dimension. The crystalline correlation lengths of the three α-$Co(OH)_2$ materials were calculated using the Scherrer[22] formula. The crystalline correlation length was largest for **II** (441 Å) followed by compounds **I** (350 Å) and **III** (185 Å).

The electron diffraction (ED) patterns in Fig. 2 mirror the respective crystalline correlation lengths calculated from the XRD data, showing large single crystals for **II** and decreasing crystallite size in **I** and **III**. Slight imperfections and possible double diffraction are observed for **I** and higher polycrystallinity is observed for **III** (Fig. 2). Narrow line widths in the XRD and single crystal ED patterns of **II** suggest that each layer is in alignment with neighboring layers and not randomly oriented around the *c*-axis.[15,23] The polycrystallinity of **I** may be due to the stacking order of the cobalt-containing sheets being parallel and equidistant but rotationally translated with respect to one another.[24] The sulfate-containing material is the most defective of the three, resulting in the observation of polycrystalline rings in the ED. Single crystal diffraction patterns were observed for **II** down the (01−1) zone axis, with *d*-spacings corresponding to the lattice planes (110), (112), and (123) (a = 3.13 Å; c = 9.19 Å). The calculated unit cell parameters for **I**, **II**, and **III** are $a_{\mathbf{I,II,III}}$ = 3.14 Å; $c_{\mathbf{I}}$ = 8.12 Å; $c_{\mathbf{II}}$ = 9.19 Å; and $c_{\mathbf{III}}$ = 11.26 Å, which are in perfect agreement with the XRD data. Unit cell dimensions obtained by the two techniques are thus identical, indicating that the material is homogeneous on the crystalline and bulk length scales.

XRD and electron diffraction data agree with one another, and indicate that the material is structurally similar to $Zn_5(OH)_8(NO_3)_2\cdot 2H_2O$.[21] This latter material is known to consist of layered sheets with octahedrally coordinated Zn ions in the brucite layer, one quarter of which are replaced by two tetrahedrally coordinated Zn ions located above and below the plane of the octahedrally coordinated Zn ions. This structure thus exhibits an overall ratio of 3 : 2 octahedral to tetrahedral sites and a charged cation layer. The same crystal structure has been previously proposed by Kurmoo for $Co_2(OH)_3(NO_3)$, $Co_5(OH)_8(O_2CC_6H_4CO_2)\cdot 2H_2O$, $Co_4(OH)_2(O_2CC_6H_4CO_2)_3\cdot (NH_3)_{1.5}(H_2O)_{2.5}$ and $Co_5(OH)_8(NO_3)_2\cdot 2H_2O$.[10] More recently, Forster *et al.* synthesized another α-cobalt hydroxide, $Co_7(OH)_{12}(C_2H_4S_2O_6)(H_2O)_2$, in which one sixth of the octahedrally coordinated Co^{2+} are replaced by two tetrahedral sites.[25]

The compositions of the α-$Co(OH)_2$ films **I**, **II** and **III** were analyzed using ICP-AES and C, H, N analysis. Based on these results, compound **I** is proposed to be $Co_5(OH)_8Cl_2{\cdot}3H_2O$ (anal. found: H, 2.70%; Co, 52.9%; calc.: H, 2.54%; Co, 53.0%). Compound **II** was found to have the composition known from the literature as $Co_5(OH)_8(NO_3)_2{\cdot}2H_2O$[16] (anal. found: H, 2.51%; N, 4.73%; Co, 52.7%; calc.: H, 2.05%; N, 4.74%; Co 49.9%) and is a direct analog of $Zn_5(OH)_8(NO_3)_2{\cdot}2H_2O$.[21] ICP-AES analysis of **III** gave a Co : S ratio of 5 : 1 and analyses are consistent with a formula of $Co_5(OH)_8SO_4{\cdot}2H_2O$ (anal. found: H, 2.29%; S, 5.91%; Co 51.8%; calc.: H, 2.15%; S, 5.70%; Co 52.4%).

X-Ray photoelectron spectroscopy (XPS) data indicate the presence of Co^{2+} with the 2p peak centred at 780.6 eV (Fig. 3a) in all three materials. The peak position and shape are consistent with literature values reported for $Co(OH)_2$.[26,27] Also these data restrict the potential presence of Co^{3+} centers to a few mol%. The O 1s peaks for all materials have a maximum intensity component centered at 530.8 eV (data not shown). This is in good agreement with previously reported data for β-$Co(OH)_2$.[26,27] The XPS data of the respective counterions for compounds **I** (Cl^-), **II** (NO_3^-) and **III** (SO_4^{2-}) are shown in Fig. 3b. All observed binding energy values are in good agreement with corresponding reference spectra (Cl $2p_{Cl}$ = 198–200;[28] N $1s_{NO3}$ = 407–408 eV;[28] S $2p_{SO4}$ = 168–171 eV[28]).

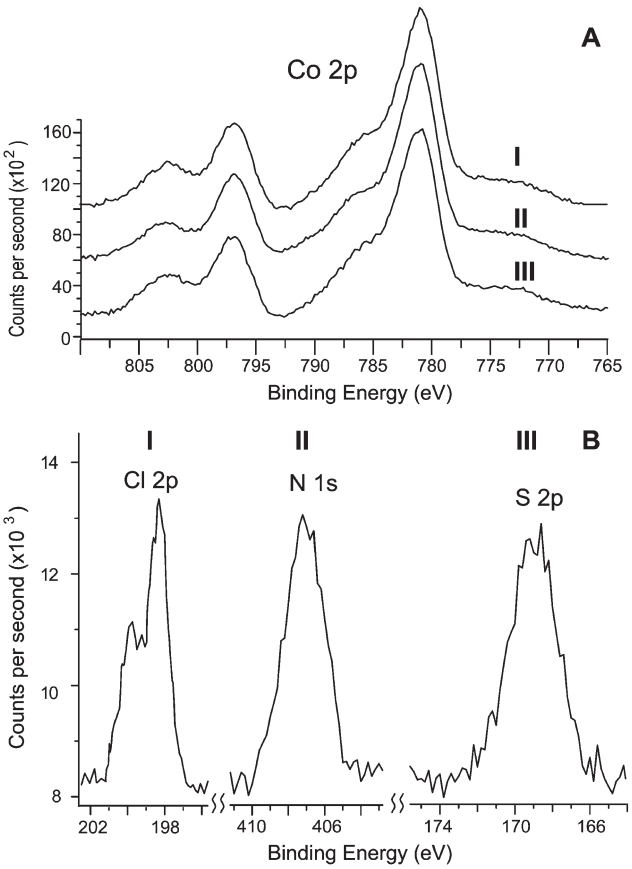

Fig. 3 High resolution XPS spectra of (A) Co 2p region for **I**, **II**, and **III** and (B) Cl 2p, N 1s and S 2p regions for **I**, **II**, and **III** respectively.

The $Co_5(OH)_8Cl_2{\cdot}3H_2O$ (**I**), $Co_5(OH)_8(NO_3)_2{\cdot}2H_2O$ (**II**) and $Co_5(OH)_8SO_4{\cdot}2H_2O$ (**III**) films are dark green in color, with visible absorption (UV/Vis) spectra showing strong peaks near 660 and 600 nm (Fig. 4) for all materials. Compound **I** absorbs at slightly higher wavelengths compared to **II**, while the spectrum of **III** is marginally blueshifted. Absorption above ~600 nm in the visible spectrum is indicative of tetrahedral Co^{2+} centers.[29] Possible features indicating octahedral Co^{2+} centers are obscured by the diffuse reflectance of the samples below 600 nm.[10,29] In contrast, β-$Co(OH)_2$ with symmetric octahedral bonding geometry around the cobalt center is pink in color (λ_{max} = 470 nm).[15]

These UV/Vis observations provide strong confirmation that our materials indeed contain tetrahedrally coordinated Co^{2+} ions. No bands indicating the presence of Co^{3+} ions could be seen. In combination with our XPS data, this supports the suggestion that the positive net charge in these α-$Co(OH)_2$ materials indeed originates from differently coordinated metal ions (as described above) instead of mixed valence ions.

X-Ray absorption near edge structure (XANES) was recorded for $Co_5(NO_3)_2(OH)_8{\cdot}2H_2O$ (**II**). The K-edge energy is 7719 eV, which is in agreement with reported values for Co(II) reference compounds.[10] A weak pre-edge feature is observed at 7709 eV. This pre-edge feature results from a lack of inversion symmetry in crystal sites due to the presence of tetrahedral coordination of some of the cobalt ions present in the material, supporting the above conclusions.

Methods used previously to make α-$Co(OH)_2$ materials involved electrochemical,[15] chemical,[19,26] and sonication assisted synthesis routes,[13,14] but direct electronic measurements previously could not be carried out on the resulting materials because of the low quality powder morphology, low crystallinity and the absence of suitable thin films. Few publications report the growth of $Co(OH)_2$ thin films on substrates. In most cases the material described was either β-$Co(OH)_2$,[30] or it is extremely amorphous,[31] with the

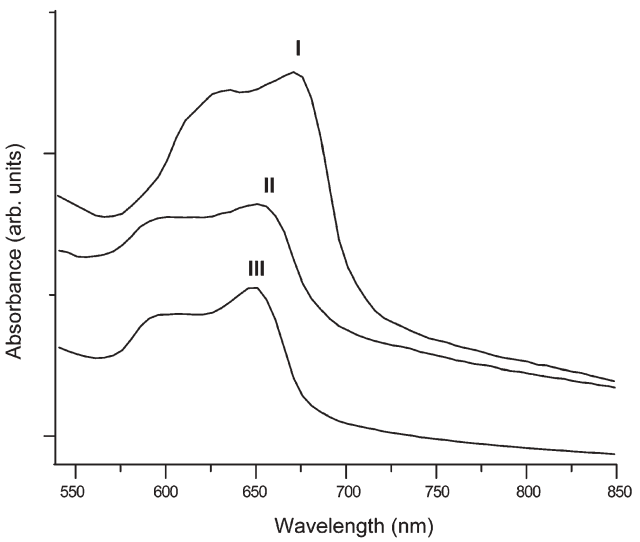

Fig. 4 Visible absorption spectra for **I**, **II**, and **III** showing two absorption maxima for each material at: **I** = 664, 622 nm; **II** = 646, 602 nm and **III** = 643, 596 nm.

exception of the thin film study by Hosono *et al.*[9] α-$Co(OH)_2$ has been investigated primarily in nanocrystalline morphology. In contrast, the continuous morphology of the films reported here makes such direct electronic measurements possible for the first time.

The continuous morphology and high degree of crystallinity of $Co_5(NO_3)_2(OH)_8{\cdot}2H_2O$ (**II**) made this material the best choice for further electronic characterization. Ohmic contact with a metallic conductor is readily achieved with physical contact between **II** and a platinum interdigitated microelectrode without the need for annealing or alloying, as evident in the observed linear response to voltage in the *IV* curve (data not shown). The *IV* characteristics were measured parallel to the plane of the material and the dark sheet resistance was observed to be ~100 Ω cm. A high anion density within the material, resulting from the interlayer incorporation of anions into the crystal structure, is consistent with the observed resistivity assuming that the contact resistance is small with respect to the bulk material resistance.[32]

We measured the photoconductive properties of **II** in view of the unique electronic environment around the cobalt centers created by the mixture of octahedrally and tetrahedrally coordinated ions in close proximity. The material is expected to behave as a p-type semiconductor because of the additional positive charge induced in the cobalt-containing layers by the replacement of one octahedral Co^{2+} site with two tetrahedral Co^{2+} sites in the crystal lattice. p-Type semiconductors exhibit an increase in conductivity when irradiated with light of sufficient energy to excite charge carriers in the material.[33] Light of energy greater than the material's band gap (E_g) generates an equal number of electrons and holes. In a p-type material this results in a large increase in concentration of minority carriers (*i.e.* electrons), thereby changing the conductivity of the material.[34] The absorption spectrum indicates that the material absorbs strongly in the visible, and therefore should be photoactive in this range of the spectrum.

We see that conductivity of the material increases sharply when exposed to visible light as a result of the increase in minority carriers (Fig. 5). After the light is turned off the minority carrier concentration decreases as $\exp(-t/\tau)$, where τ is the minority carrier lifetime. The observed decay curve is fit to a single exponential (Fig. 5 dark grey line) with $\tau = 4.8$ s and $R^2 = 0.991$. This high quality fit to a single exponential is an indication that one process dominates the decay of the conductivity response; it is in good agreement with the above physical characterization indicating relatively defect-free crystallinity. These results suggest that the material behaves as a highly doped p-type semiconductor with a long minority carrier lifetime and a degree of crystallinity sufficient for low resistance conduction. The apparent high doping concentration is most likely a result of the counter anions between the crystalline sheets of $Co(OH)_2$. The unusually long minority carrier lifetime is consistent with the large single crystal domains observed by XRD and ED.

Diffraction and analytical methods similar to those described above were used to confirm the structures of the $Cu_2(OH)_3(NO_3)$, $Zn_5(OH)_8(NO_3)_2{\cdot}2H_2O$ and $Mn_3(PO_4)_2{\cdot}7H_2O$ thin films. Properties of these materials will be reported elsewhere.

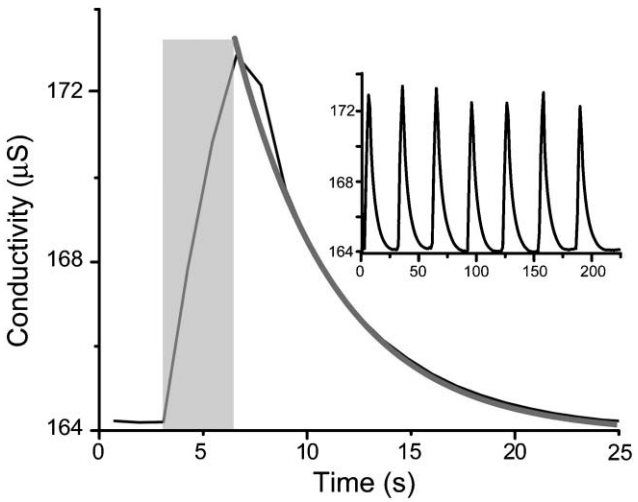

Fig. 5 Observation of photoconductive behavior of **II** on a platinum interdigitated micro-electrode with 2 s light pulses (grey box represents duration of time light is on) from a fiber optic visible light source (spectral range of 400–1400 nm with an intensity of 80×10^3 lux) and 2.5 V applied bias. Dark grey line represents an exponential curve fit to the data $\tau = 4.8$ s ($R^2 = 0.991$). Inset shows reproducibility of the photoconductive response over an extended time course (200 s).

Conclusions

Using a kinetically and spatially controlled vapor-diffusion process, we have synthesized a variety of nanostructured metal hydroxide and metal phosphate thin films at ambient temperature and pressure. Most of these materials have not been reported in thin film morphology before.

Our template-free large area films allow for the first time characterization of films in which the electronic properties and crystal structure are not influenced by the presence of a substrate. The layered $Co_5(NO_3)_2(OH)_8{\cdot}2H_2O$ material produced by this method exhibits a high degree of crystallinity and unique electronic properties. Characterization of photoconductive properties shows a weak photoconductive response and indications of a long minority carrier lifetime (4.8 s) and high doping density within the material. The observed photoconductive response is not very intense, but considering that this behavior has not been observed before for α-$Co(OH)_2$, our observations support the suggestion that this low-temperature solution-based synthesis of inorganic thin films described here may provide an important new route to materials synthesis to facilitate the characterisation of electrochemical properties of both known and new materials.

Although it is not yet known whether the materials described here may be useful for large-scale applications, the methodology for synthesis that we report is versatile and the materials described here are simply first examples of thin films grown by this vapor-diffusion mechanism. As we have shown, the process is generic and not limited to metal hydroxide synthesis. We have observed that the as-synthesized thin films can be dehydrated and converted to the respective metal oxide films with no change in morphology by heating in air. It may therefore be widely useful for room temperature fabrication of semiconducting films based on a variety of other materials.

Acknowledgements

We thank Sam Webb at SSRL for his help with the aquisition of the XANES spectra. We thank A. K. Cheetham, T. Mates and J. C. Weaver for their helpful suggestions. This work was supported in part by grants from the U.S. Dept. of Energy, DARPA, the U.S. Army Research Office (Institute for Collaborative Biotechnologies), NASA (University Research, Engineering and Technology Institute on Bio Inspired Materials (BIMat)), the NOAA National Sea Grant College Program, U.S. Department of Commerce through the California Sea Grant College System, and the MRSEC Program of the National Science Foundation (UCSB Materials Research Laboratory). Portions of this research were carried out at the Stanford Synchrotron Radiation Laboratory, a national user facility operated by Stanford University on behalf of the U.S. Department of Energy, Office of Basic Energy Sciences. The SSRL Environmental Remediation Science Program is supported by the Department of Energy, Office of Biological and Environmental Research. The U.S. Government is authorized to reproduce and distribute copies for governmental purposes.

References

1 C. N. R. Rao, G. U. Kulkarni, V. V. Agrawal, U. K. Gautam, M. Ghosh and U. Tumkurkar, *J. Colloid Interface Sci.*, 2005, **289**, 305.
2 J. H. Fendler, *Nanoparticles and nanostructured films, preparation, characterization and application*, Wiley-VCH, Weinheim, 1998.
3 Y. A. Vlasov, X.-Z. Bo, J. C. Sturm and D. J. Norris, *Nature*, 2001, **414**, 289.
4 M. Ch. Lux-Steiner, A. Ennaoui, Ch.-H. Fischer, A. Jäger-Waldau, J. Klaer, R. Klenk, R. Könenkamp, Th. Matthes, R. Scheer, S. Siebentritt and A. Weidinger, *Thin Solid Films*, 2000, **361–362**, 533.
5 S. Marian, D. Tsiulyanu, T. Marian and H.-D. Liess, *Pure Appl. Chem.*, 2001, **73**, 2001.
6 J. L. Sumerel, W. Yang, D. Kisailus, J. C. Weaver, J. H. Choi and D. E. Morse, *Chem. Mater.*, 2003, **15**, 4804.
7 D. Kisailus, J. H. Choi, J. C. Weaver, W. Yang and D. E. Morse, *Adv. Mater.*, 2005, **17**, 314.
8 D. E. Morse, *Trends Biotechnol.*, 1999, **17**, 230.
9 E. Hosono, S. Fujihara, I. Honma and H. Zhou, *J. Mater. Chem.*, 2005, **15**, 1938.
10 M. Kurmoo, *Chem. Mater.*, 1999, **11**, 3370.
11 V. Pralong, A. Delahaye-Vidal, B. Beaudoin, B. Gérand and J. M. Tarascon, *J. Mater. Chem.*, 1999, **9**, 955.
12 F. Bardé, M.-R. Palacin, B. Beaudoin, A. Delahaye-Vidal and J.-M. Tarascon, *Chem. Mater.*, 2004, **16**, 299.
13 P. Jeevanan, Y. Koltypin, A. Gedanken and Y. Mastai, *J. Mater. Chem.*, 1999, **9**, 511.
14 Y. Zhu, H. Li, Y. Koltypin and A. Gedanken, *J. Mater. Chem.*, 2002, **12**, 729.
15 R. S. Jayashree and P. V. Kamath, *J. Mater. Chem.*, 1999, **9**, 961.
16 M. Kurmoo, *Philos. Trans. R. Soc. London, Ser. A*, 1999, **357**, 3041.
17 G. H. Chen, Z. S. Hu, J. X. Dong, L. G. Wang, Y. Peng, T. He and R. Lai, *Lubr. Eng.*, 2001, **57**, 36.
18 P. Elumalai, H. N. Vasan and N. Munichandraiah, *J. Power Sources*, 2001, **93**, 201.
19 M. Rajamathi, P. V. Kamath and R. Seshadri, *Mater. Res. Bull.*, 2000, **35**, 271.
20 P. V. Kamath and G. H. A. Therese, *J. Solid State Chem.*, 1997, **128**, 38.
21 W. Stählin and H. R. Oswald, *Acta Crystallogr., Sect. B*, 1970, **26**, 860.
22 G. S. Hammond, *An introduction to crystallography and diffraction*, Oxford University Press, Oxford, 1998.
23 K. T. Ehlsissen, A. Delahaye-Vidal, P. Genin, M. Figlarz and P. Wiliams, *J. Mater. Chem.*, 1993, **3**, 883.
24 B. D. Cullity, *Elements of X-Ray Diffraction*, 2nd edn, Addison-Wesley, Reading, MA, 1978.
25 P. M. Forster, M. M. Tafoya and A. K. Cheetham, *J. Phys. Chem. Solids*, 2004, **65**, 11.
26 J. Haber and L. Ungier, *J. Electron Spectrosc. Relat. Phenom.*, 1977, **12**, 305.
27 J. Haber, J. Stoch and L. Ungier, *J. Electron Spectrosc. Relat. Phenom.*, 1976, **9**, 459.
28 J. F. Moulder, W. F. Stickle, P. E. Sobol and K. D. Bomben, *Handbook of X-ray Photoelectron Spectroscopy*, ed. J. Chastain and R. C. King, Physical Electronics, Eden Praire, MN, 1995.
29 A. B. P. Lever, *Inorganic Electronic Spectroscopy*, 2nd edn, Elsevier, New York, 1984, pp. 480–505.
30 J. Ismail, M. F. Ahmed and P. V. Kamath, *J. Power Sources*, 1991, **36**, 507.
31 N. Özer, D.-G. Chen and T. Büyüklimanli, *Sol. Energy Mater. Sol. Cells*, 1998, **52**, 223.
32 ASTM F723-99.
33 J. Mort and D. M. Pai, *Photoconductivity and related phenomena*, Elsevier, New York, NY, 1976.
34 J. D. Livingston, *Electronic Properties of Engineering Materials*, Wiley, New York, NY, 1999.